Crystal Structure of Recombinant Farnesyl Diphosphate Synthase at 2.6-Å Resolution[†,Δ]

L. C. Tarshis,[‡] Mujing Yan,[§] C. Dale Poulter,*[,§] and James C. Sacchettini*[,‡]

Department of Biochemistry, Albert Einstein College of Medicine, 1300 Morris Park Avenue, Bronx, New York 10461, and Department of Chemistry, University of Utah, Salt Lake City, Utah 84112

Received June 6, 1994; Revised Manuscript Received July 13, 1994[•]

ABSTRACT: The synthesis of farnesyl diphosphate (FPP), a key intermediate in the isoprenoid biosynthetic pathway required for the synthesis of cholesterol and in the formation of prenylated proteins, is catalyzed by the enzyme farnesyl diphosphate synthase (FPS). The crystal structure of avian recombinant FPS, the first three-dimensional structure for any prenyltransferase, was determined to 2.6-Å resolution. The enzyme exhibits a novel fold composed entirely of α-helices joined by connecting loops. The enzyme's most prominent structural feature is the arrangement of 10 core helices around a large central cavity. Two aspartate-rich sequences that are highly conserved among the isoprenyl diphosphate synthase family of prenyltransferases, and are essential for enzymatic activity, were found on opposite walls of this cavity, with the aspartate side chains approximately 12 Å apart and facing each other. The location and metal ion binding properties of these sequences suggest that the conserved aspartate residues participate in substrate binding or catalysis.

The isoprenoid biosynthetic pathway, with over 23 000 metabolites, is unrivaled elsewhere in nature for the chemical diversity of the compounds it produces. Farnesyl diphosphate (FPP) is a key intermediate that serves as a substrate for several important branch-point enzymes. In humans, FPP is required for the first committed steps in the biosynthesis of cholesterol (Zhang et al., 1993), farnesylated proteins (Clark, 1992), geranylgeranylated proteins (Clark, 1992), ubiquinones (Ashby, 1990a), dolichols (Matsuoka, 1991), and heme *a* (Weinstein et al., 1986). Because of their importance to health, considerable effort has been devoted to finding inhibitors for the synthesis of cholesterol and prenylated proteins involved in tumorigenesis. FPP is constructed from isopentenyl diphosphate (IPP) and dimethylallyl diphosphate (DMAPP) as shown in Scheme 1.

Avian FPS is typical of the enzymes that synthesize FPP. The enzyme is a homodimer of 44-kDa subunits, each of which contains a single active site. The chain elongation reaction proceeds in two distinct steps. IPP and DMAPP are condensed to form GPP, which serves as the allylic substrate for a second condensation with IPP to produce FPP (Poulter & Rilling, 1978). Binding studies indicate that the active site contains distinct allylic and homoallylic binding domains (Reed & Rilling, 1975, 1976) and suggest that the E-GPP-PP_i complex formed upon condensation of IPP and DMAPP must rearrange to expel PP_i and reposition GPP before the second reaction. The mechanism of this rearrangement has not been firmly established. FPS is a member of a larger family of isoprenoid diphosphate synthases that catalyze chain elongation by prenyl transfer to IPP. Those that synthesize FPP and geranylgeranyl diphosphate (GGPP) appear to have similar structures (Chen et al., 1994). The longer chain isoprenyl diphosphate synthases are less well characterized, and some may have different quaternary structures.

Scheme 1

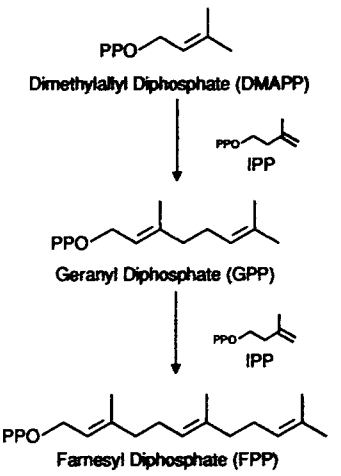

While there is a relatively modest level of amino acid sequence similarity throughout the family, all isoprenyl diphosphate synthases contain five conserved regions, two of which include DDXXD or DDXXXXD motifs (Ashby et al., 1990, 1991, 1992). Site-directed mutagenesis experiments (Joly & Edwards, 1993; Song & Poulter, 1994) indicate that all the aspartates in the first aspartate-rich region (D117–D121), as well as two nearby arginines (R126 and R127), are important for catalysis. They also showed that, in the second Asp-rich region (D257–D261), the first two aspartates appear to be more important than the third. Otherwise, little is known about the three-dimensional structures of the enzymes involved in cholesterolgenesis. We describe here the crystal structure of recombinant avian FPS at 2.6-Å resolution.

EXPERIMENTAL PROCEDURES

Crystallization. Avian liver FPS was expressed in *Escherichia coli* using procedures described for the yeast enzyme (Song & Poulter, 1994) and purified to homogeneity as described by Reed and Rilling (1976). Crystals were obtained by hanging drop/vapor diffusion, using the 50-point sparse scan method (Jancarik & Kim, 1991). Small crystals

[†] This work was supported by National Institutes of Health Grants GM45859 (J.C.S.), 5T32 GM07260 (L.C.T.), and GM21328 (C.D.P.).

[Δ] Coordinates for the crystal structure of farnesyl diphosphate synthase have been deposited with the Brookhaven Protein Data Bank under the filename 1FPS.

* Correspondence should be addressed to either author.

[‡] Albert Einstein College of Medicine.

[§] University of Utah.

[•] Abstract published in *Advance ACS Abstracts*, August 15, 1994.

0006-2960/94/0433-10871$04.50/0

Table 1

data set	resolution (Å)	% complete	no. of unique	redundancy	R_{merge}[a] (%)	R_{iso}[b] (%)	fractional coordinates X	Y	Z
native	2.13	80.1	25 159	2.9	11.5				
DMA	2.37	67.4	27 648	3.1	9.1	12.4	0.0354	0.1475	0.0339
Sm	2.72	73.4	20 563	2.2	8.1	17.0	0.1447	0.4636	0.1138
							0.2287	0.3880	0.1188
DMA/Sm	2.37	69.2	28 482	2.9	11.4	19.9	same as above		
HgI	2.39	68.6	28 552	2.9	9.5	9.6	0.0352	0.1472	0.0339
PCMPS	2.72	93.2	22 742	3.7	15.7	18.2	0.0314	0.1802	0.0223
							0.1262	0.2465	0.0937

resolution (Å)	DMA phasing power[c]	Sm phasing power	DMA/Sm phasing power	HgI phasing power	PCMPS phasing power	combined figure of merit[d]
9.0	2.67	1.07	1.27	1.77	1.18	0.915
6.0	2.83	1.12	1.45	1.95	1.23	0.890
5.0	2.55	1.04	1.37	1.77	1.16	0.830
4.5	2.37	1.00	1.33	1.65	1.14	0.785
4.0	2.15	0.96	1.33	1.53	1.14	0.724
3.5	1.87	0.93	1.32	1.38	1.18	0.590
3.0	1.55	0.92	1.34	1.24	1.23	0.460
2.7	0.57	0.78	1.36	1.15	1.26	0.360
av	2.19	0.98	1.31	1.51	1.12	0.691

[a] $R_{merge} = 100\,(\sum_h\sum_i|\langle I(\vec{h}_i)\rangle - I(\vec{h}_i)|/\sum_h\sum_i I(\vec{h}_i))$, where $\langle I(\vec{h}_i)\rangle$ is the average of symmetry equivalents. [b] $R_{iso} = 100(\sum_{\vec{h}}|I_{PH}(\vec{h}) - I_P(\vec{h})|/\sum_{\vec{h}}|I_{PH}(\vec{h}) + I_P(\vec{h})|)$, where I_{PH} and I_P are derivative and native intensities, respectively. [c] Phasing power $= |\langle F(\vec{h})\rangle|/E$, where $\langle F(\vec{h})\rangle$ and E = average structure factor and lack of closure error, respectively. [d] FOM: $\bar{F}_P(\vec{h}) = (\int \bar{F}_P(\vec{h})P(\varphi)\,d\varphi)/(\int P(\varphi)\,d\varphi)$.

were first observed at an FPS concentration of 18 mg/mL in 0.8 M tartrate and 0.1 M Hepes, pH 8.4. Conditions were optimized to produce crystals with a maximum size of 0.4 × 0.9 mm at various protein and precipitant concentrations and pH values. Typical optimum conditions were 20 mg/mL FPS in 0.78 M tartrate, 0.1 M Hepes, and 20 mM phosphate, at pH 6.5. Crystals were also prepared at these conditions in the presence of 1–1.5 mM IPP. Additionally, crystals prepared in the absence of IPP were later soaked in mother liquor solutions (without phosphate) containing 1–5 mM IPP and 1 mM $MgCl_2$ or moved into 0.83 M ammonium sulfate–0.1 M Hepes, containing the same concentrations of IPP and $MgCl_2$.

Data Collection and Space Group Determination. Crystals were irradiated at room temperature with a Rigaku RU200 rotating anode X-ray generator, and data were collected with a Siemens Model X1000 area detector. The collection distance was 14–20 cm. Diffraction data were processed with XENGEN software (Howard, 1986). The unit cell dimensions and space group were determined by using XENGEN and the pseudo precession program PRECESS (Furey & Swaminathan, 1990). The protein was found to crystallize in the tetragonal space group $I4_122$, with unit cell dimensions of $a = b = 89.2$ Å and $c = 276.0$ Å and one monomer per asymmetric unit. Assuming the average value of 0.74 cm^3/g for the protein-specific volume, a value of 63% solvent was obtained for the unit cell.

Structure Determination and Refinement. Electron density maps were obtained by multiple isomorphous replacement (MIR) methods. Over thirty heavy atom compounds were used in the search for isomorphous derivatives. Diffraction-quality crystals were obtained from 14 of these compounds. Four of these produced the one double- and four single-site derivative data sets used in the final MIR phasing. All the mercurial compounds tested produced cracks in the crystals, and it was necessary to incubate the soluble protein with the mercurials before crystallization. The resulting crystals were isomorphous with native crystals. A clear samarium (Sm) derivative was only obtained after transferring the crystals out of the tartrate mother liquor and into 0.83 M ammonium sulfate. Removal of the chelating tartrate ML (K_d of ≈0.01 M for Mg^{2+} and ≈10^{-6} M for Sm^{3+}) was necessary to produce Sm derivatives. The four compounds used in the derivatives chosen for MIR phasing were dimercuric acetate (DMA), mercuric iodide (HgI), *p*-(chloromercuri)benzenesulfonic acid (PCMPS), and samarium acetate (Sm). The double derivative was prepared by soaking a DMA cocrystal in Sm containing ammonium sulfate ML. All derivative data collection scans were set up to maximize collection of anomalous diffraction reflections. The heavy atom sites were confirmed with the VERIFY program (S. Roderick, unpublished) which was also used to search for secondary sites. The PHASES software (Furey & Swaminathan, 1990) was used for protein phasing and to determine the correct hand of the molecule by using the anomalous data from the derivatives. The recommended 3σ cutoff for reflections was used. Phasing was also done using a 2σ and 1σ sigma data cutoff, but these maps were judged to be of lower quality by visual inspection. Results of the data collection and phasing are shown below in Table 1. The resulting 2.7-Å resolution electron density maps were clear enough to allow tracing most of the chain without the addition of any model phase information. The α-helices could easily be seen, and most of the side chains were visible. The TOM software (Jones, 1985) was used for model building. The chain was built from alanine residues and continued until all the visible helical regions were fit. The many well-defined side chains helped to unambiguously fix the directions of most of the helices. Approximately 200 alanine residues, or 55% of the total, were fit before model phases were calculated. Structure factors computed from the model were combined with the MIR phases, and new maps were calculated. The combined phase maps allowed additional residues to be fit to the ends of helices and improved the electron density in the loop regions. Additional improvements in the maps were obtained by extending the phases to include reflections rejected by PHASES, by using the SQUASH software (Main, 1990). The sequence assignment showed which residues bound the heavy atoms. They were PCMPS1 = Cys98, PCMPS2 = Cys72, DMA = HgI = Cys161, Sm1 = Asps117/121, and Sm2 = Asps257/261. The sequence assignment enabled the rest of the chain to be built, with the exception of the sections containing residues 1–17, 264–279, and 290–320. These

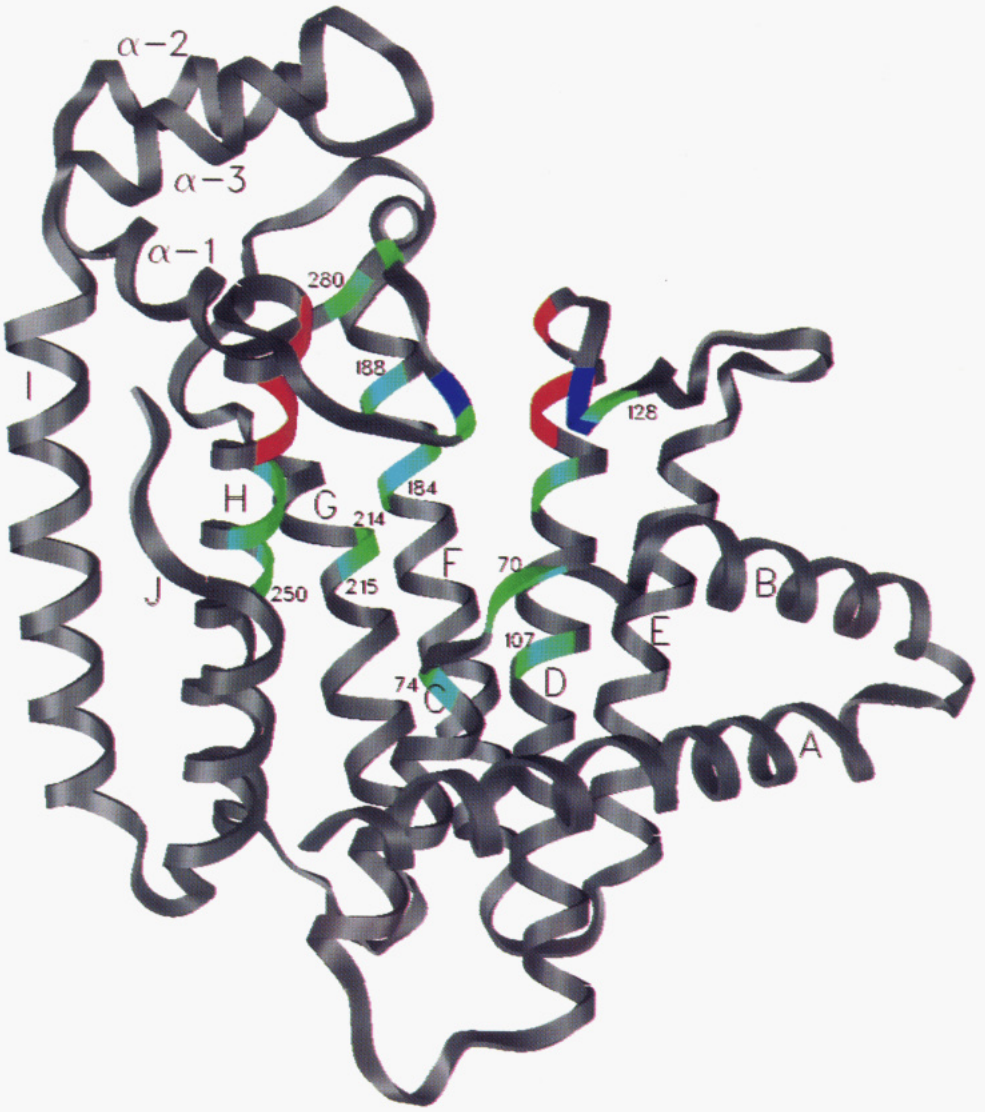

FIGURE 1: Structure of FPS, illustrating the five sequences (70–74, 107–128, 184–188, 214–215, and 250–280) containing residues conserved in 13 members of the isoprenyl diphosphate synthase family. These sequences were found to line the cavity containing the substrate binding sites. The conserved residues are shown in greenish blue. The two conserved DDXXD sequences (D117–D121 and D257–D261) are shown with the aspartate residues in red. The conserved essential basic residues (R126, R127, and K271) are shown in dark blue. The helical segments are labeled A–J and contain the following residues: A = 23–46, B = 53–66, C = 73–85, D = 94–119, E = 142–158, F = 167–191, G = 205–229, H = 237–262, α-1 = 284–289, α-2 = 296–303, α-3 = 310–320, I = 325–346, and J = 352–363. Figure prepared with SETOR.

regions showed little or no electron density. The partial structure was refined with XPLOR (Brünger et al., 1987), using dynamic simulation followed by Powell energy minimization, to a resolution of 2.7 Å. Several iterations of phase-combination, model rebuilding with difference and omit maps, followed by refinements, allowed the completion of the 290–320 stretch. Repetition of this process with the additional residues added allowed the 264–279 segment to be built. After the addition of 78 water molecules, the structure was refined to a resolution of 2.6 Å. The data between 2.6 and 2.1 Å were not included, for two reasons. First, the completeness of the data fell off dramatically from the value of 79% obtained at 2.6 Å. Second, reflections with resolution greater than 2.6 Å were much weaker and had significantly lower I/σ values than the lower resolution reflections. The final refinement produced an R-factor of 19.4%, an average B-factor, over all atoms, of 38.9, and rms deviations from canonical geometry of 0.012 Å in bond lengths and 1.70° in bond angles.

RESULTS AND DISCUSSION

Overall Structure. Recombinant avian FPS has an all-α-helix (and loop) structure with a previously unreported folding pattern (Figure 1). The structure shows the protein folded as a single domain, whose major structural feature is a core composed of 10 α-helices. These 10 α-helices are antiparallel in the +1, +1, +1, +1 topology described by Richardson (1981) and appear as three distinct layers, or sheets, as viewed in Figure 1. The first layer is formed by α-helices A and B, the second contains J, C, D, and E, and the third layer is formed by F, G, H, and I. The axes of the helices of sheets 2 and 3 are somewhat aligned, giving them a stacked appearance, while the two helices of the first layer (A and B) are nearly orthogonal to the stack. Each of the 10 helices of the core shows extensive hydrophobic interactions with a neighboring helix of similar length in such a way that the paired helices run nearly antiparallel. Helices D and H are located in the center of the protein's core and contain the DDXXD sequences shown by mutagenesis (Joly, 1993; Song, 1994) to be important in binding and catalysis. Helix D is buried and forms interactions with helices A, B, C, E, F, and G. Helix H forms a slightly twisted pair of α-helices with helix G and is further stabilized by van der Waals contacts made with the hydrophobic residues of helices I and J.

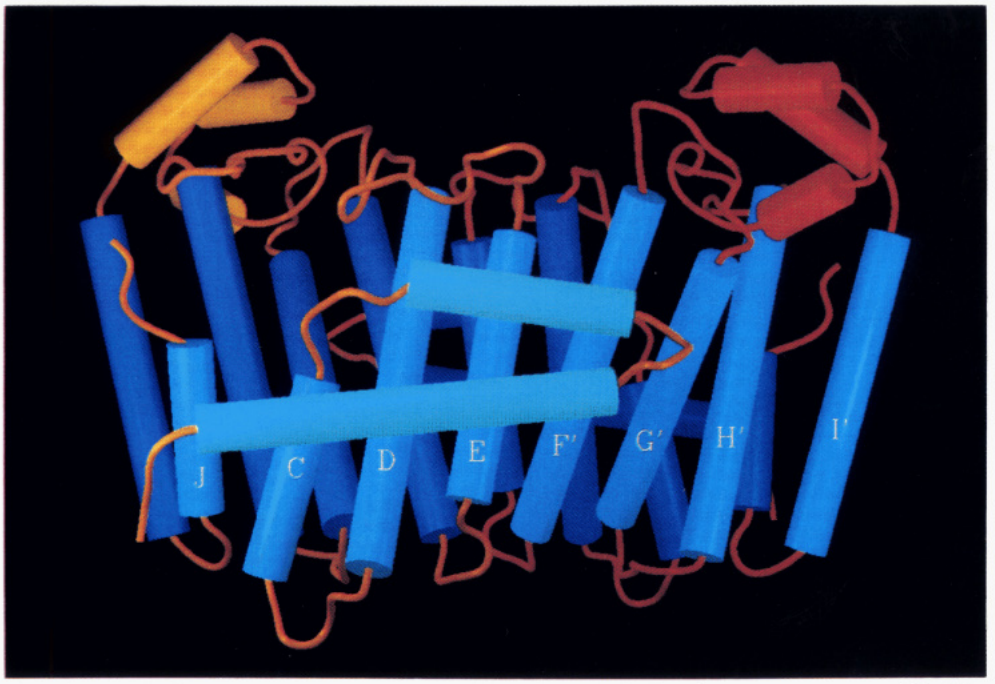

FIGURE 2: Illustration of the FPS dimer with α-helices represented by tubes. The helices from monomer 1 are joined by gold loops. Loops in monomer 2 are colored magenta. The 2-fold dimer axis is in the plane of the paper, approximately vertical, and in between helices E and F′. The four helix layers are shown in different shades of blue, with the first layer (front) in the lightest shade. Layer 4 (back) is the darkest. The extended layer 2 is labeled to show the four helices contributed by layer 2 of monomer 1 (J, C, D, and E) and the four contributed from layer 3 of monomer 2 (F′, G′, H′, and I′). Figure prepared with SETOR.

This layered helical arrangement results in a long and flat protein with dimensions of approximately 65 × 65 × 35 Å. At the lower end of the helical stack, as viewed in Figure 1, the interconnecting loops between the helices are relatively short. These loops are all less than nine residues in length and contain glycine, proline, and/or asparagine residues, amino acids typically present in tight turns. At the opposite end of the stack (the top as viewed in Figure 1), the connecting loops are significantly longer, ranging between 13 and 60 amino acids. These longer loops do not contain any extended regular secondary structure elements (i.e., α-helices or β-strands), with the exception of the loop between helices H and I. This loop, formed by residues 265–323, is the longest of the interhelix connections. It contains 21 residues that are in extended conformation followed by 3 short α-helices, α-1, α-2, and α-3, which spiral to the top of the protein as viewed in Figure 1. The few interactions that these short helices form with the core structure come from van der Waals contacts between hydrophobic side chains of helix α-3 and residues in loop F–G and helix I. These three α-helices are weakly stabilized by van der Waals contacts between hydrophobic side chains within the cluster.

The core helices of the enzyme surround a large deep cleft, measuring approximately 14 × 18 × 18 Å in width, height, and depth, respectively, as viewed in Figure 1. The two short α-helices in the central layer, J and C, form the floor of the cleft. The back wall of the cleft is lined by helices F and G, while the sides are formed by helices D and H. The roof of the cleft is formed by the loops between helices D–E and H–I. The interior surface of the cavity contains four deep depressions, and its volume is 2382 Å^3, as determined from GRASP calculations (Nichols & Honig, 1990). In comparison, the total molecular volume of the enzyme is 51 465 Å^3. The cleft is lined with the side chains of 16 hydrophobic, 14 polar, and 15 ionizable amino acids that contribute approximately 22%, 18%, and 60% of the 1500-Å^2 total cavity surface area, respectively. The ionizable residues are clustered into patches of intense positive and negative charge, while the others are more dispersed.

Structure of the FPS Dimer. Avian FPS is active as a homodimer (Reed, 1976). The organization of the molecules in the crystal lattice indicated that the dimer occurs in solution in the orientation shown in Figure 2. A Connolly algorithm calculation of the contact surfaces, using a 1.4-Å probe radius, showed that the buried area for this arrangement was 1029 Å^2 of the 5696 Å^2 total surface area. In addition, this pairing of subunits results in a large number of hydrophobic contacts at the dimer interface. There are 6 aromatic and 17 hydrophobic residues from each subunit buried at the interface. Many of the side chains from these residues are extended into the interface and form van der Waals contacts with side chains from the other subunit.

The subunits of the dimer are related by a perfect 2-fold axis that is approximately coincident with the axis that defines α-helices D and E (see Figure 2). This orientation places helices D and E at the center of the dimer interface where they produce about 550 Å^2 of the interface surface. The dimer structure aligns the pseudoplanes of the second helical layer of one subunit with the third helical layer of the other subunit, thereby elongating the two layers to form sheets that contain eight α-helices each. Additional interactions between the subunits arise from the helix–turn–helix sequence (α-A–α-B), which is tightly packed against the two central sheets in the dimer and contributes 11 hydrophobic side chains. This extends the orthogonal helix–sheet interaction formed in each subunit and completes the tertiary structural motif by creating a symmetrical structure consisting four helix–sheets.

The FPS Active Site Is Located in the Large Central Cavity. Sequence alignments have identified five regions with highly conserved amino acids in 13 members of the isoprenyl diphosphate synthase family (Chen & Poulter, 1994). As shown in Figure 1, the highly conserved amino acids in these sequences are all located in the immediate vicinity of the deep cleft that forms the putative substrate binding pocket. Two

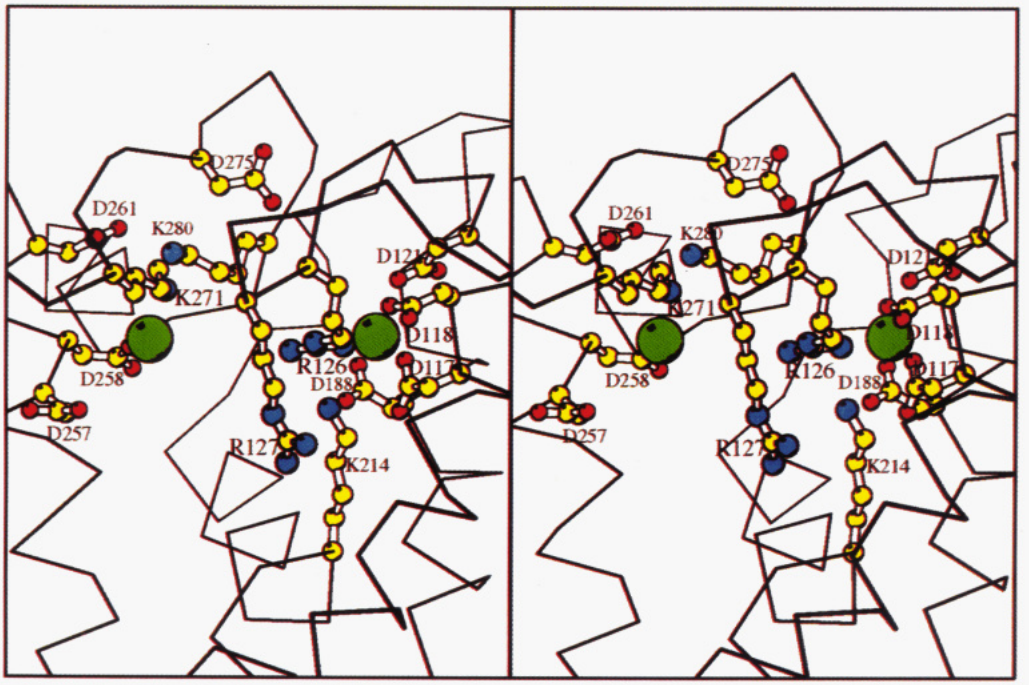

FIGURE 3: Stereoview of the FPS active site cavity. Each of the two conserved DDXXD sequences (D117–D121 and D257–D261) binds one samarium atom (in green). Also shown are the conserved basic residues (R126, R127, and K271) found downstream from the DDXXD sequences. Additional acidic and basic residues that are in proximity to the proposed substrate binding sites are also shown. Figure prepared by MOLSCRIPT.

of the longer sequences contain DDXXD motifs common to many prenyltransferases (Chen & Poulter, 1994). In avian FPS the first aspartate-rich region (D117–D118–I119–M120–D121) has conserved arginines (R126 and R127) downstream, while the second aspartate-rich region (D257–D258–Y259–L260–D261) has a conserved lysine (K271). Ashby et al. (1990b) proposed that the aspartates in these regions bind the diphosphate moieties of the substrates through Mg^{2+} bridges. Mutagenesis studies (Joly & Edwards, 1993; Song & Poulter, 1994) confirmed the importance of the aspartates and arginines in the first region and residues D257 and D258 in the second. Song and Poulter showed that substitution of the charged side chains in amino acids with uncharged moieties decreased k_{cat} by 5–7 orders of magnitude. In contrast, substitutions for D261 and K271 gave only 6–16-fold reductions.

In the three-dimensional structure of avian FPS, the aspartate-rich sequences are located near the C-terminal end of α-helix D and α-helix H, respectively. The side chains of aspartates 117, 118, 121, 257, 258, and 261 are positioned so their carboxylate groups all point into the cleft. This alignment places each Asp-rich sequence on opposite sides of the upper walls of the cleft as viewed in Figure 3. The location of these residues lends support to the above mentioned hypothesis (Ashby & Edwards, 1990) and corroborating mutagenesis studies (Joly & Edwards, 1993; Song & Poulter, 1994). It is likely that the mutations in these aspartate residues produced their effects from the direct interference with residues involved in substrate binding or catalysis, rather than from structural changes that alter the geometry of other ligand binding sites of FPS. Further evidence for the involvement of these residues in substrate binding or catalysis came from samarium heavy atom derivatives. A samarium binding site is located in each of the two Asp-rich conserved regions (Figure 3), placing the two sites about 10 Å apart. Because samarium can bind to the Mg^{2+} binding site of enzymes (Needham et al., 1993), we postulate that samarium binds to the substrate–Mg^{2+} binding sites. Additionally, the configuration of the carboxylate clusters, each containing three Asps, is similar to the Mg^{2+} binding clusters observed in many phosphotransfer enzymes, nucleases, and phospho-regulated proteins (Needham et al., 1993). Typically there are 3–4 carboxyl groups coordinating one side of the Mg^{2+} ion, with 2–3 waters completing the coordination sphere on the other side of the ion. It is presently unclear if, in FPS, all three carboxyl groups in each cluster participate in coordinating the Mg^{2+} ions. The conserved basic residues located downstream from the DDXXD motifs are found in the loops between helices D and E and helices H and I. The side chains of these residues (Arg126, Arg127, and Lys271) also extend into the cleft near the side chains of the conserved aspartate residues, suggesting that they may form electrostatic or hydrogen-bonding interactions with the diphosphate moieties of the substrates or be involved in base-assisted catalysis. The molecular surface topography and associated relative charge distribution near the cleft are illustrated in Figure 4.

Volume calculations of the cleft and substrate molecules show that the substrates occupy only a small part of the cleft. For example, the calculated volume of 195 $Å^3$ for an IPP molecule is less than one-tenth of the cavity volume. Low-resolution difference ($|F_o| - |F_c|$) maps prepared from crystals soaked in IPP–Mg^{2+}–tartrate or IPP–Mg^{2+}–sulfate showed two positive electron density peaks next to each of the two conserved Asp sequences in the cavity, but they were not resolved sufficiently at this resolution to enable the unambiguous placement of IPP molecules within the active site. Additionally, the weak electron density observed may reflect partial occupancy of IPP due to inhibition by tartrate or sulfate in the mother liquors. However, the electron density peaks were each large enough to accommodate an IPP molecule, and both envelopes were located immediately adjacent to one of the pairs of conserved Asps. Preliminary model building, using IPP molecules in their minimum energy states, showed that, by placing the ligands in the observed difference density, they could be positioned in an orientation that permits formation of GPP from IPP and DMAPP.

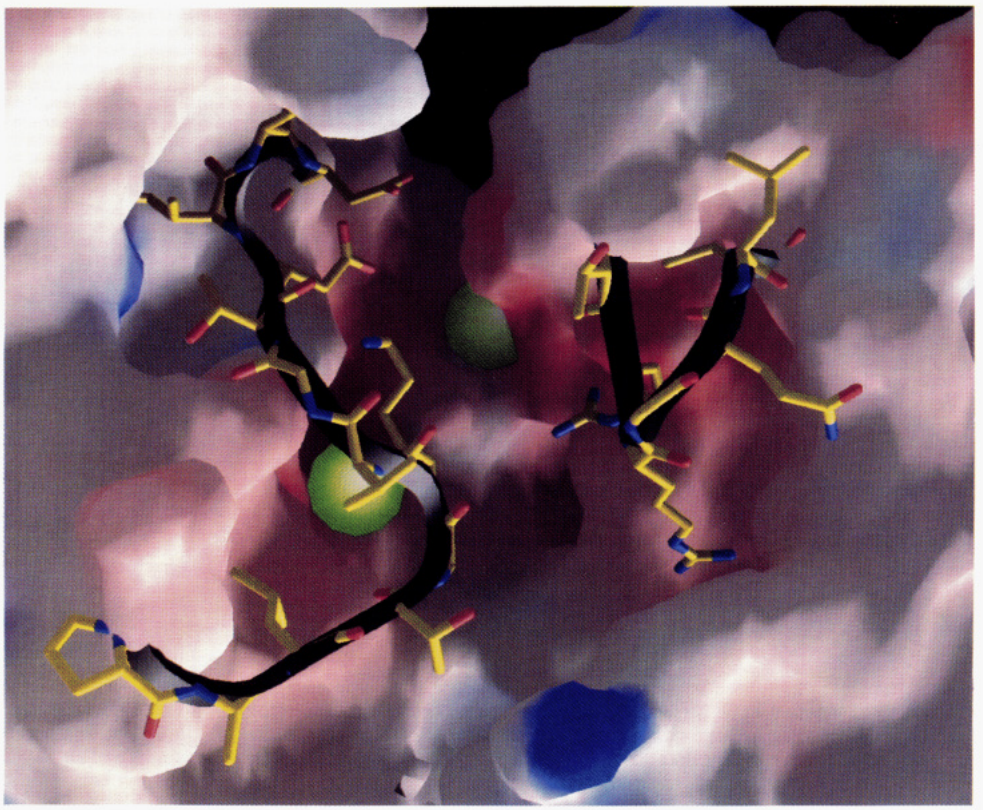

FIGURE 4: Magnified view of the substrate binding site cavity showing the molecular surface topography and associated potential. Negative potential is shown in red and positive in blue. The surface contributed by residues T125–L130 (right loop) and P266–D278 (left loop) has been excluded to make the inside of the cavity visible. The two bound samarium atoms are shown as green spheres. The conserved basic residues associated with the two essential DDXXD sequences (R126, R127, and K271) are visible in the exposed loops. The surface was constructed using a 1.4-Å probe radius and assigned relative charge values by setting the charge parameters of Lys-NZ = 1.0, Arg-NH1 and -NH2 = 0.5, Glu-OE1 and -OE2 =–0.5, and Asp-OD1 and -OD2 = –0.5. Figure prepared with GRASP.

This preliminary assignment of the E·2IPP complex gave a structure with the diphosphate moieties located adjacent to the aspartate-rich regions on opposite sides of the cavity and the hydrocarbon chains sandwiched in between. This overall orientation is compatible with the stereochemical studies of Davisson and Poulter (1993), using bisubstrate analogs to determine the topology of IPP and DMAPP in the enzyme–substrate complex. However, the location of the hydrocarbon chains is not consistent with the stereochemistry of the condensation between IPP and DMAPP (Poulter & Rilling, 1978). Reed and Rilling (1976) found that avian FPS binds a single molecule of DMAPP, K_d = 1.8 μM, or GPP, K_d = 0.17 μM, per subunit in the presence of Mg^{2+}. In contrast, two molecules of IPP are bound under similar conditions, and one is displaced upon addition of citronilyl diphosphate, a nonreactive GPP analog. In the absence of Mg^{2+}, only one IPP binds per monomer, with a $K_d \approx 4$ μM (Rilling, 1979).

The location of the two IPPs in the crystal structure leaves the hydrocarbon residues exposed to water within the cavity. Since the carbocationic species formed during catalysis are highly reactive electrophiles, they must be shielded from solvent. This could most logically be accomplished by a conformational change of the 264–288 loop upon binding the Mg^{2+} salts of IPP and the allylic diphosphate that positions the substrates deeper in the cavity. This loop is flexible, as indicated by its weak electron density and high thermal factors. In addition, there are three glycine residues (264, 270, and 273) that would aid in the movement of the loop. The proposed movement also brings the conserved Lys271 closer to the substrates. Finally, the rate constants for addition of IPP and allylic diphosphate to avian FPS are considerably below the diffusion-controlled limit, and it was suggested that a conformational change may accompany substrate binding (Laskovics & Poulter, 1981).

REFERENCES

Ashby, M. N., & Edwards, P. A. (1990) *J. Biol. Chem. 265*, 13157–13164.

Ashby, M. N., Spear, D. H., & Edwards, P. A. (1990) *Proceedings of the 20th Steenbeck Symposium* (Attie, A. D., Ed.) pp 27–35, Elsevier, New York.

Brünger, A. T., Kuriyan, J., & Karplus, M. (1987) *Science 235*, 458–460.

Chen, A., & Poulter, C. D. (1994) *Protein Sci. 3*, 600–607.

Clarke, S. (1992) *Annu. Rev. Biochem. 61*, 355–386.

Furey, W., & Swaminathan, S. (1990) *Am. Crystallogr. Assoc. Mtg. Prog. Abstr. 18*, 73.

Howard, A. J. (1986) *The XENGEN System*, Protein Engineering Department, Genex Corp., Gaithersburg, MD.

Jancarik, J., & Kim, S. H. (1991) *J. Appl. Crystallogr. 24*, 409–411.

Joly, A., & Edwards, P. A. (1993) *J. Biol. Chem. 268*, 26983–26989.

Jones, T. A. (1985) *Methods Enzymol. 115*, 157–171.

Laskovics, F. M., & Poulter, C. D. (1981) *Biochemistry 20*, 1893–1901.

Main, P. (1990) *Acta Crystallogrr. A46*, 372–377.

Matsuoka, S., Sagami, H., Kurisaki, A., & Ogura, K. (1991) *J. Biol. Chem. 266*, 3464–3468.

Needham, J. V., Chen, T. Y., & Falke, J. J. (1993) *Biochemistry 32*, 3363–3367.

Nichols, A., & Honig, B. (1990) *GRASP*, Columbia University, New York.

Poulter, C. D., & Rilling, H. C. (1978) *Acc. Chem. Res. 11*, 307–313.

Reed, B., & Rilling, H. C. (1975) *Biochemistry 14*, 51–54.
Reed, B., & Rilling, H. C. (1976) *Biochemistry 15*, 3739–3745.
Richardson, J. S. (1981) *Adv. Protein Chem. 34*, 167–339.
Rilling, H. C. (1979) *Pure Appl. Chem. 51*, 597–608.
Song, L., & Poulter, C. D. (1994) *Proc. Natl. Acad. Sci. U.S.A. 91*, 3044–3048.
Weinstein, J. D., Branchard, R., Berle, S. I., Bement, W. J., & Sinclair, P. R. (1986) *Arch. Biochem. Biophys. 245*, 44–50.
Yoshida, I., Koyama, T., & Ogura, K. (1987) *Biochemistry 26*, 6840–6845.
Zhang, D., Jennings, S. M., Robinson, G. W., & Poulter, C. D. (1993) *Arch. Biochem. Biophys. 304*, 133–143.